Snakes and Ladders: Localized Solutions of Plane Couette Flow

Tobias M. Schneider,[1] John F. Gibson,[2] and John Burke[3]

[1]School of Engineering and Applied Sciences, Harvard University, 29 Oxford Street, Cambridge, Massachusetts 02138, USA
[2]School of Physics, Georgia Institute of Technology, 837 State Street, Atlanta, Georgia 30332, USA
[3]Department of Mathematics and Statistics, Boston University, Boston, Massachusetts 02215, USA

(Received 14 December 2009; published 8 March 2010)

We demonstrate the existence of a large number of exact solutions of plane Couette flow, which share the topology of known periodic solutions but are localized in one spatial dimension. Solutions of different size are organized in a snakes-and-ladders structure strikingly similar to that observed for simpler pattern-forming partial differential equations. These new solutions are a step towards extending the dynamical systems view of transitional turbulence to spatially extended flows.

DOI: 10.1103/PhysRevLett.104.104501 PACS numbers: 47.54.−r, 47.27.ed

The discovery of exact equilibrium and traveling-wave solutions to the full nonlinear Navier-Stokes equations has resulted in much recent progress in understanding the dynamics of linearly stable shear flows such as pipe, channel, and plane Couette flow [1–4]. These exact solutions, together with their entangled stable and unstable manifolds, form a dynamical network that supports chaotic dynamics, so that turbulence can be understood as a walk among unstable solutions [5,6]. Moreover, specific exact solutions are found to be edge states [7], that is, solutions with codimension-1 stable manifolds that locally form the stability boundary between laminar and turbulent dynamics. Thus, exact solutions play a key role both in supporting turbulence and in guiding transition.

This emerging dynamical systems viewpoint does not yet capture the full spatiotemporal dynamics of turbulent flows. One major limitation is that exact solutions have mostly been studied in small computational domains with periodic boundary conditions. The small periodic solutions cannot capture the localized structures typically observed in spatially extended flows. For example, pipe flows exhibit localized turbulent puffs. Similarly, in plane Couette flow (PCF), the flow between two parallel walls moving in opposite directions, localized perturbations trigger turbulent spots which then invade the surrounding laminar flow [8,9]. Both localized turbulence and even more regular long-wavelength spatial patterns such as turbulent stripes have been observed [10]. The known periodic exact solutions cannot capture this rich spatial structure, but they do suggest that localized solutions might be key in understanding the dynamics of spatially extended flows.

Spatially localized states are common in a variety of driven dissipative systems. These are often found in a parameter regime of bistability (or at least coexistence) between a spatially uniform state and a spatially periodic pattern, such as occurs in a subcritical pattern-forming instability. The localized state then resembles a slug of the pattern embedded in the uniform background. An early explanation of such states is due to Pomeau [11], who argued that a front between a spatially uniform and spatially periodic state, which might otherwise be expected to drift in time, can be stabilized over a finite parameter range by pinning to the spatial phase of the pattern. More recently, the details of this localization mechanism have been established for the subcritical Swift-Hohenberg equation (SHE) through a theory of spatial dynamics [12–14]. In one spatial dimension the time-independent version of this PDE can be treated as a dynamical system in space, in which stationary profiles are seen as trajectories in the spatial coordinate. Then localized states correspond to homoclinic orbits to a fixed point that visit the neighborhood of a periodic orbit representing the pattern. The SHE is equivariant under spatial reflections, so the corresponding spatial dynamical system is reversible. There exists an infinite multiplicity of reversible homoclinic orbits (i.e., symmetric localized states) organized in a pair of solution branches which undergo homoclinic snaking. In a bifurcation diagram the two branches intertwine, oscillating back and forth within a parameter regime called the snaking or pinning region. These are connected by branches of nonsymmetric states called rungs. Together they form the snakes-and-ladders structure of localized states.

The theory of spatial dynamics also applies to other equations in one spatial dimension [15], but there is no obvious extension to higher dimensional PDEs. Nevertheless, there are remarkable similarities between localized states in the simple one-dimensional SHE and in other more realistic (and complicated) PDEs. In fluid dynamics, homoclinic snaking occurs in driven two-dimensional systems such as binary fluid convection [16] and natural doubly diffusive convection [17]. Localized solutions in these systems exhibit snaking in bifurcation diagrams and are homoclinic in that they transition along one of the spatial coordinates from a uniform state, to a periodic pattern, and back to the uniform state. In three-dimensional shear flows, homoclinic snaking has never

been observed but its existence has been speculated [18]. This speculation is supported by the recent discovery of two localized exact solutions in PCF by Schneider, Marinc, and Eckhardt [19] which qualitatively resemble localized states in the SHE.

The aim of this Letter is to elucidate the origin of these localized solutions in PCF. We show that the Navier-Stokes equations in this geometry indeed exhibit homoclinic snaking, giving rise to localized counterparts of well-known spatially periodic equilibria.

In PCF the velocity field $\mathbf{u}(\mathbf{x}, t) = [u, v, w](x, y, z, t)$ evolves under the incompressible Navier-Stokes equations,

$$\frac{\partial \mathbf{u}}{\partial t} + \mathbf{u} \cdot \nabla \mathbf{u} = -\nabla p + \frac{1}{\mathrm{Re}} \nabla^2 \mathbf{u}, \qquad \nabla \cdot \mathbf{u} = 0, \quad (1)$$

in the domain $\Omega = L_x \times L_y \times L_z$ where x, y, z are the streamwise, wall-normal, and spanwise directions, respectively. The boundary conditions are periodic in x and z and no-slip at the walls, $\mathbf{u}(y = \pm 1) = \pm \hat{\mathbf{x}}$. The Reynolds number is $\mathrm{Re} = Uh/\nu$, where U is half the relative velocity of the walls, h half the wall separation, and ν the kinematic viscosity. We treat Re as the control parameter and use as a solution measure the dissipation rate $D = (L_x L_y L_z)^{-1} \int_\Omega (|\nabla \times \mathbf{u}|^2) d\Omega$. The laminar profile has $D = 1$ while solutions such as those shown in Fig. 1 have $D > 1$.

Figure 1 shows two exact solutions of (1) at $\mathrm{Re} = 400$ and $\Omega = 4\pi \times 2 \times 16\pi$, originally identified in [19] for $\Omega = 4\pi \times 2 \times 8\pi$. The solutions are localized in the spanwise z direction and consist of two to three prominent pairs of alternating wavy roll-streak structures embedded in a laminar background flow. Figures 1(a) and 1(b) are a traveling-wave solution $\mathbf{u}_{\mathrm{TW}}$ of (1) satisfying $[u, v, w](x, y, z, t) = [u, v, w](x - c_x t, y, z, 0)$, where $c_x = 0.028$ is the streamwise wave speed. Figures 1(c) and 1(d) are a stationary, time-independent solution $\mathbf{u}_{\mathrm{EQ}}$. The equilibrium $\mathbf{u}_{\mathrm{EQ}}$ is symmetric under inversion $[u, v, w](x, y, z, t) = [-u, -v, -w](-x, -y, -z, t)$, and the traveling-wave $\mathbf{u}_{\mathrm{TW}}$ has a shift-reflect symmetry, $[u, v, w](x, y, z, t) = [u, v, -w](x + L_x/2, y, -z, t)$. These symmetries ensure that neither $\mathbf{u}_{\mathrm{EQ}}$ nor $\mathbf{u}_{\mathrm{TW}}$ drifts in the localization direction z.

To continue these solutions in Re, we combine a Newton-Krylov hookstep algorithm [20] with quadratic extrapolation in pseudoarclength along the solution branch. The Navier-Stokes equations are discretized with a Fourier-Chebyshev-tau scheme in primitive variables and 3rd-order semi-implicit backwards differentiation time stepping. Bifurcations along the solution branches are characterized by linearized eigenvalues computed with Arnoldi iteration. The computations were performed with $32 \times 33 \times 256$ collocation points and 2/3-style dealiasing, resulting in approximately 2×10^5 free variables, and validated by recomputing with $(3/2)^3$ more grid points at a number of locations along each solution curve [21].

The bifurcation diagram in Fig. 2 shows the $\mathbf{u}_{\mathrm{TW}}$ and $\mathbf{u}_{\mathrm{EQ}}$ solutions from Fig. 1 under continuation in Reynolds number. As Re decreases below 180, the solution branches

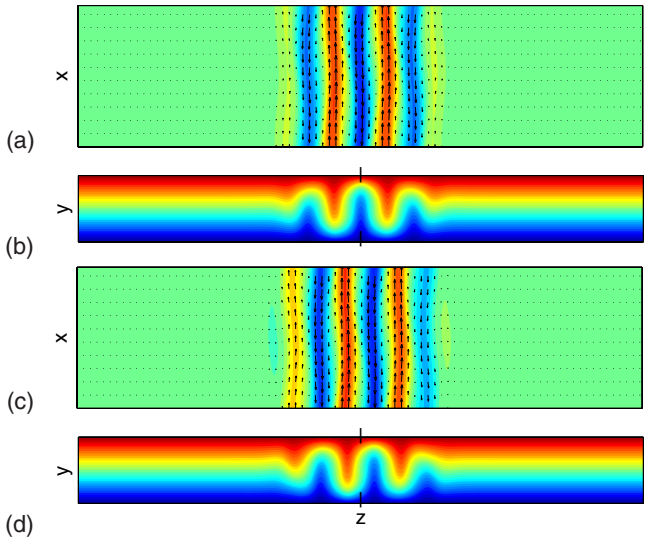

FIG. 1 (color online). Localized traveling-wave $\mathbf{u}_{\mathrm{TW}}$ (a),(b) and equilibrium $\mathbf{u}_{\mathrm{EQ}}$ (c),(d) solutions of plane Couette flow at $\mathrm{Re} = 400$, from [19]. The velocity fields are shown in the $y = 0$ midplane in (a),(c), with arrows indicating in-plane velocity and the color scale indicating streamwise velocity u: dark, light, dark (blue, green, red) correspond to $u = -1, 0, +1$. The x-averaged streamwise velocity is shown in (b),(d), with y expanded by a factor of 3.

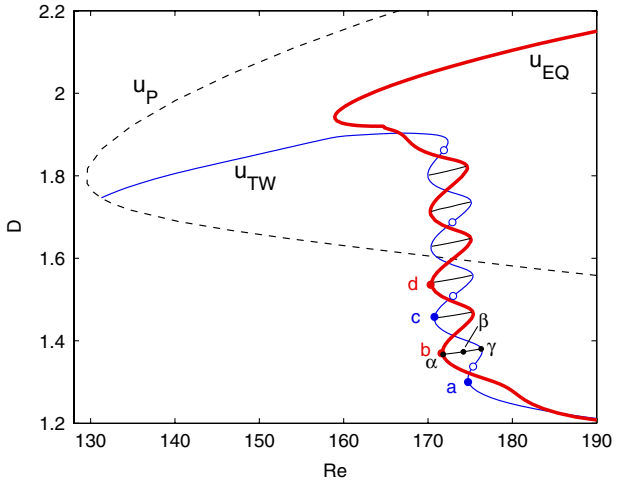

FIG. 2 (color online). Snaking of the localized $\mathbf{u}_{\mathrm{TW}}$, $\mathbf{u}_{\mathrm{EQ}}$ solutions of plane Couette flow in (Re, D) plane. The spatially periodic Nagata solution $\mathbf{u}_P$ is shown as well; the $\mathbf{u}_{\mathrm{TW}}$ solution connects with it near (131, 1.75). Velocity fields of the localized solutions at the saddle-node bifurcations labeled a, b, c, d are shown in Fig. 3. The rung branches are shown with solid lines connecting the $\mathbf{u}_{\mathrm{EQ}}$ and $\mathbf{u}_{\mathrm{TW}}$ in the snaking region; velocity fields for the points marked α, β, γ are shown in Fig. 4. Open dots on the $\mathbf{u}_{\mathrm{TW}}$ traveling-wave branch mark points at which the wave speed passes through zero.

snake upwards in dissipation D; that is, they pass through a sequence of sub- and supercritical saddle-node bifurcations which nearly line up, creating a large multiplicity of localized solutions in $169 < \mathrm{Re} < 177$. Each saddle-node bifurcation adds structure at the edges (fronts) of the localized solution while preserving its symmetry. This spatial growth is illustrated in Fig. 3, which shows the velocity fields at several points along the snaking branches. For example, Fig. 3(a) shows the $y = 0$ midplane of $\mathbf{u}_{\mathrm{TW}}$ at the saddle-node bifurcation marked a in Fig. 2. Continuing up the solution branch from (a) to (c), the solution gains a pair of streaks at the fronts while the interior structure stays nearly constant. The marginal eigenfunction associated with the saddle-node bifurcation at (c) is shown in Fig. 3(g); it is weighted most heavily at the fronts of the localized solution and has the same symmetry, so that adding a small component of the eigenfunction strengthens and slightly widens the fronts, whereas subtraction weakens and shrinks them.

The spanwise wavelength of the interior structure of the localized solutions is approximately $\ell_z \approx 7$. This value is selected by the fronts that connect the interior streaks to the laminar background, and it does not seem to vary much across the snaking region or when compared between the two branches. The streamwise wave speed c_x of the traveling-wave solution varies along the branch and in fact changes sign several times. Points at which $c_x = 0$ are marked in Fig. 2 with open circles. The point marked (a) has $c_x = 0.0062$. Rotation about the z axis generates symmetric partners for both $\mathbf{u}_{\mathrm{TW}}$ and $\mathbf{u}_{\mathrm{EQ}}$; for the former this results in a streamwise drift in the opposite direction. Thus the $\mathbf{u}_{\mathrm{TW}}$ and $\mathbf{u}_{\mathrm{EQ}}$ curves in Fig. 2 represent four solution branches. The lower branches of both can be continued upwards in Reynolds number past $\mathrm{Re} = 1000$.

Figure 2 also shows six rungs of nonsymmetric exact localized solutions. These bifurcate from the snaking branches close to the saddle nodes and are associated with marginal eigenfunctions whose symmetry does not match the base state. Each rung connects to both the $\mathbf{u}_{\mathrm{EQ}}$ and the $\mathbf{u}_{\mathrm{TW}}$ branch so solutions along the rungs smoothly interpolate between the two symmetry subspaces, as illustrated in Fig. 4. The rung solutions travel in z as well as x, but with z wave speed 3 orders of magnitude smaller than c_x.

Because of the finite extent of the domain, the structures cannot grow indefinitely, and the snaking behavior must terminate. As in other problems of this type, the details of this termination depend on a commensurability condition between the spanwise wavelength of the streaks within the localized solutions and the spanwise domain [22]. At $L_z = 16\pi$, $\mathbf{u}_{\mathrm{TW}}$ connects at $(\mathrm{Re}, D) = (131, 1.75)$ to the spatially periodic Nagata equilibrium with wavelength $\ell_z = 2\pi$. The $\mathbf{u}_{\mathrm{EQ}}$ branch does not appear to connect to any periodic solution. Instead, when this branch exits the snaking region its velocity field contains a localized defect that persists under continuation up to at least $\mathrm{Re} = 300$. At other values of L_z, both branches might either not connect to a periodic solution or connect to a different periodic solution. For example, in Ref. [19] it was shown that at $L_z = 8\pi$ both the $\mathbf{u}_{\mathrm{TW}}$ and $\mathbf{u}_{\mathrm{EQ}}$ branches terminate on a branch of spatially periodic solutions, though that choice of L_z was too narrow to allow the snaking structure to develop.

We have shown that homoclinic snaking in wide plane Couette channels gives rise to a family of exact localized

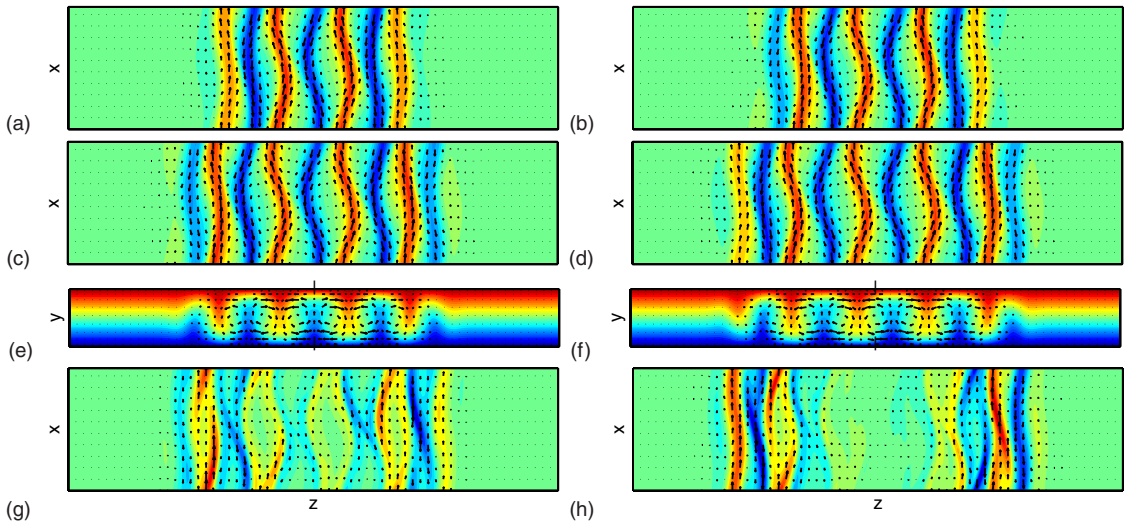

FIG. 3 (color online). Localized traveling-wave $\mathbf{u}_{\mathrm{TW}}$ (left) and equilibrium $\mathbf{u}_{\mathrm{EQ}}$ (right) solutions of plane Couette flow at points marked on the solution branches in Fig. 2. (a),(c) show the velocity fields of $\mathbf{u}_{\mathrm{TW}}$ at its first and second saddle-node bifurcations, moving up each branch from lower to higher dissipation D; similarly (b),(d) for $\mathbf{u}_{\mathrm{EQ}}$. (e),(f) show the x-averaged velocity of (c),(d), with in-plane velocity indicated by arrows and streamwise velocity by the color map as in Fig. 1. The marginal eigenfunctions at the saddle-node bifurcations (c),(d) are shown in (g),(h).

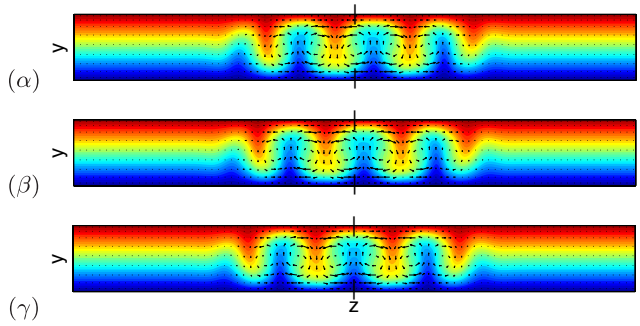

FIG. 4 (color online). Localized solutions of plane Couette flow along a rung branch, for the points marked α, β, γ in Fig. 2, and plotted in terms of x-averaged streamwise velocity $\langle \mathbf{u} \rangle_x(y, z)$ as in Figs. 1(b) and 1(d). (α) shows the beginning of the rung solution on the $\mathbf{u}_{\mathrm{EQ}}$ branch with symmetry $\langle \mathbf{u} \rangle_x(y, z) = -\langle \mathbf{u} \rangle_x(-y, -z)$. Midway along the rung, (β) is nonsymmetric. The rung terminates at (γ) on the $\mathbf{u}_{\mathrm{TW}}$ branch with symmetry $\langle \mathbf{u} \rangle_x(y, z) = \langle \mathbf{u} \rangle_x(y, -z)$.

solutions with internal structure similar to the periodic Nagata equilibrium. Thus, as recently speculated [18,19], the localization mechanism studied in the SHE carries over to linearly stable shear flows, where it cannot be associated with an instability of the uniform state [23]. Physically, the localized states studied above consist of fronts pinned to the periodic Nagata equilibrium. The periodic structure is formed by pairs of counterrotating, streamwise-oriented roll-streak structures, which also characterize other exact solutions linked to transitional turbulence in small domains. Therefore, localized versions of the other known exact solutions should also exist and, together with their heteroclinic connections, support localized turbulence. In this sense the localized solutions studied here are a first step towards generalizing the dynamical systems picture for turbulence to extended flows.

Turbulent spots and stripes that are tilted against the flow direction suggest the existence of fully localized exact solutions, i.e., solutions localized in both the spanwise and streamwise directions. Although a theory for localization in two spatial dimensions is not yet available, numerical studies of the SHE show that snaking does carry over to solutions localized in two dimensions [24]. In PCF it is, however, not known if the same mechanism also generates fully localized exact solutions because a bifurcation analysis would first require a fully localized solution to start the continuation. Such a solution is unfortunately not yet available. Nevertheless, edge calculations both in pipe flow [25,26] and in extended plane Couette cells [19,27,28] yield localized structures that show very mild dynamic fluctuations, which suggests the existence of simple underlying fully localized exact solutions.

We would like to thank Edgar Knobloch for helpful discussions and Predrag Cvitanović and Bruno Eckhardt for helpful comments on the manuscript. T. M. S. was supported by German Research Foundation Grant No. Schn 1167/1. J. F. G. was supported by NSF Grant No. DMS-0807574. J. B. was supported by NSF Grant No. DMS-0602204.

[1] M. Nagata, J. Fluid Mech. **217**, 519 (1990).
[2] F. Waleffe, J. Fluid Mech. **435**, 93 (2001).
[3] H. Faisst and B. Eckhardt, Phys. Rev. Lett. **91**, 224502 (2003).
[4] H. Wedin and R. R. Kerswell, J. Fluid Mech. **508**, 333 (2004).
[5] O. E. Landford, Annu. Rev. Fluid Mech. **14**, 347 (1982).
[6] J. F. Gibson, J. Halcrow, and P. Cvitanović, J. Fluid Mech. **611**, 107 (2008).
[7] T. M. Schneider, J. F. Gibson, M. Lagha, F. De Lillo, and B. Eckhardt, Phys. Rev. E **78**, 037301 (2008).
[8] N. Tillmark and P. H. Alfredsson, J. Fluid Mech. **235**, 89 (1992).
[9] F. Daviaud, J. Hegseth, and P. Bergé, Phys. Rev. Lett. **69**, 2511 (1992).
[10] D. Barkley and L. S. Tuckerman, Phys. Rev. Lett. **94**, 014502 (2005).
[11] Y. Pomeau, Physica (Amsterdam) **23D**, 3 (1986).
[12] A. R. Champneys, Physica (Amsterdam) **112D**, 158 (1998).
[13] J. Burke and E. Knobloch, Chaos **17**, 037102 (2007).
[14] S. J. Chapman and G. Kozyreff, Physica (Amsterdam) **238D**, 319 (2009).
[15] M. Beck, J. Knobloch, D. J. B. Lloyd, B. Sandstede, and T. Wagenknecht, SIAM J. Math. Anal. **41**, 936 (2009).
[16] O. Batiste, E. Knobloch, A. Alonso, and I. Mercader, J. Fluid Mech. **560**, 149 (2006).
[17] A. Bergeon and E. Knobloch, Phys. Fluids **20**, 034102 (2008).
[18] E. Knobloch, Nonlinearity **21**, T45 (2008).
[19] T. M. Schneider, D. Marinc, and B. Eckhardt, J. Fluid Mech. **646**, 441 (2010).
[20] D. Viswanath, J. Fluid Mech. **580**, 339 (2007).
[21] The numerical software is available at www.channelflow.org.
[22] A. Bergeon, J. Burke, E. Knobloch, and I. Mercader, Phys. Rev. E **78**, 046201 (2008).
[23] V. A. Romanov, Funct. Anal. Appl. **7**, 137 (1973).
[24] D. Lloyd, B. Sandstede, A. Avitabile, and A. R. Champneys, SIAM J. Appl. Dyn. Syst. **7**, 1049 (2008).
[25] A. P. Willis and R. R. Kerswell, J. Fluid Mech. **619**, 213 (2009).
[26] F. Mellibovsky, A. Meseguer, T. M. Schneider, and B. Eckhardt, Phys. Rev. Lett. **103**, 054502 (2009).
[27] D. Marinc, Master's thesis, Philipps-Universiät Marburg, 2008.
[28] Y. Duguet, P. Schlatter, and D. S. Henningson, Phys. Fluids **21**, 111701 (2009).